

# RSC Advances



This is an *Accepted Manuscript*, which has been through the Royal Society of Chemistry peer review process and has been accepted for publication.

*Accepted Manuscripts* are published online shortly after acceptance, before technical editing, formatting and proof reading. Using this free service, authors can make their results available to the community, in citable form, before we publish the edited article. This *Accepted Manuscript* will be replaced by the edited, formatted and paginated article as soon as this is available.

You can find more information about *Accepted Manuscripts* in the [Information for Authors](#).

Please note that technical editing may introduce minor changes to the text and/or graphics, which may alter content. The journal's standard [Terms & Conditions](#) and the [Ethical guidelines](#) still apply. In no event shall the Royal Society of Chemistry be held responsible for any errors or omissions in this *Accepted Manuscript* or any consequences arising from the use of any information it contains.

# Supramolecular Assembly of Dipeptide Functionalized Benzo[ghi]perylene Monoimide Directs White Light Emission via Donor-Acceptor Interactions

*Manoj K. Manna,<sup>[a]</sup> Dnyaneshwar B. Rasale,<sup>[a]</sup> and Apurba K. Das<sup>\*[a]</sup>*

<sup>[a]</sup>Department of Chemistry, Indian Institute of Technology Indore, Indore 452017, India

\*To whom correspondence should be made

Dr. Apurba K. Das

Email: apurba.das@iiti.ac.in

**ABSTRACT**

An aromatic dipeptide Phe-Phe (FF) functionalized benzo[ghi]perylene monoimide (BPI) is synthesized and its optical behavior, self-assembly nature in different organic solvents are studied. Diels-Alder reaction of perylene and *N,N'*-maleoyl-Phe-Phe-OMe produces a new fluorophores (BPI-FF-OMe) which is highly soluble in a wide range of organic solvents without any swallow alkyl chain. The dipeptide appended benzo[ghi]perylene monoimide (BPI-FF-OMe) self-assembles into nanospheres both in methanol and toluene solvents. The nanospherical structures are driven by hydrogen bonding and  $\pi$ - $\pi$  stacking interactions among aromatic dipeptide appended benzo[ghi]perylene monoimide. Self-assembled nano-architecture of BPI-FF-OMe is studied by a number of microscopic techniques. Tunable solvent dependent photophysical behavior of BPI-FF-OMe is also studied. The synthesized BPI-FF-OMe exhibits positive solvatochromic emission ( $\lambda_{em}$  (toluene) = 508 nm;  $\lambda_{em}$  (methanol) = 566 nm) as a function of solvent polarity with higher lifetimes ( $\tau_{toluene}$  = 8.4 ns;  $\tau_{methanol}$  = 5.7 ns) and quantum yields ( $\phi_f$  = 0.55(toluene);  $\phi_f$  = 0.39(methanol)). The BPI-FF-OMe shows white light emission upon energy transfer between donor pyrenebutyric acid (PyBA) to acceptor BPI-FF-OMe molecule. In order to study the role of peptide sequence Phe-Phe attached with perylene moiety of BPI-FF-OMe molecule, an amino acid functionalized BPI-L-OMe molecule is also synthesized. BPI-L-OMe also shows white light emission upon energy transfer from donor pyrenebutyric acid (PyBA) molecules to acceptor BPI-L-OMe molecules. Benzo[ghi]perylene moiety plays an important role for energy transfer from donor pyrene moiety to acceptor benzo[ghi]perylene moiety that exhibits white light emission.

## 1. INTRODUCTION

Self-assembled  $\pi$ -conjugated perylene based amphiphiles have attracted considerable interest in recent years.<sup>1-3</sup> Self-assembled perylene based amphiphiles have been used in the fabrication of supramolecular 1D, 2D, and 3D based micro and nano-architectures for the applications in biology and supramolecular electronics.<sup>4-6</sup> A variety of perylene based molecules have been designed for the development of perylene dye chemistry through extension of perylene core via functionalizing the bay position of perylene.<sup>7-13</sup> Extensive work has been done on perylene diimides (PDI).<sup>14</sup> The stable supramolecular architectures are achieved by designing the molecular structure of self-assembled materials as well as optimizing the response of suitable stimuli.<sup>15-19</sup> Various stimuli have been used to drive the self-assembly of organic moieties via hydrogen bonding,  $\pi$ - $\pi$  stacking and hydrophobic interactions. Zang *et al.* reported several examples of PDI based self-assembly.<sup>20-22</sup> Self-assembly of amino acid functionalized perylene bisimides is also reported in literature.<sup>23-25</sup> Recently, self-assembly of peptides functionalized perylene bisimides has been reported.<sup>26-27</sup> In general, low molecular weight hydrophobic peptides have been used for the evolution of self-assembled architectures.<sup>28-32</sup> Schenning *et al.* reported mixed fluorescent co-oligomer systems for the creation of white-light-emitting gels.<sup>33</sup> Ajayaghosh *et al.* reported supramolecular organogel composed of intertwined twisted helical fibrillar assemblies made of OPPV decorated with cholesterol units.<sup>34</sup> Meijer and co-worker also described a supramolecular copolymer resulting from the self-assembly in films of blue, green, and red  $\pi$ -conjugated oligomers.<sup>35</sup> Zhang and co-workers described photo-facilitated aggregation and stable white-light emission in solution.<sup>37</sup> Zhang *et al.* also reported bright white-light emission from a novel donor-acceptor small organic molecule in the solid state via intermolecular charge transfer.<sup>38</sup> Number of strategies have been used to fabricate white light

emitting materials. These include metal mediated white light emission,<sup>39</sup> combination of three primary colors (red, green and blue), polymers<sup>40</sup> and self-assembly of organic molecules.<sup>41</sup> Development of low molecular weight white light emitting material is particularly interesting due to their good solubility in distinct solvents. They can easily be applied on solid surface or can be soaked on solid materials. There are various reports (Table S1) but none of the examples show acceptor perylene monoimide functionalized small organic molecules based white light emission upon donor-acceptor interactions. Thus, keeping all these aspects in mind, we have explored an aromatic benzo[ghi]perylene monoimide (BPI) functionalized diphenylalanine methyl ester (BPI-FF-OMe) and BPI-L-OMe for the evolution of white light emission. The BPI-FF-OMe is highly soluble in various organic solvents and shows solvchromic behavior in different solvents.

Herein, our aim is to explore self-assembly of benzo[ghi]perylene monoimide (BPI) functionalized dipeptide for the evolution of white light emission via donor-acceptor interactions. White light emitting materials have become an area of interest because of their opto-electronic applications. Till date, several research groups have emphasized the development of white light emitting materials. Acceptors benzo[ghi]perylene monoimides (BPIs) and donor pyrenebutyric acid lead to white light emission via donor-acceptor interactions. Benzo[ghi]perylene monoimide functionalized dipeptide (BPI-FF-OMe) and amino acid (BPI-L-OMe) are a new class of acceptor molecules which show white light emission with pyrene via energy transfer from donor to acceptor molecular interactions (Scheme 1).

## 2. RESULTS AND DISCUSSION

### 2.1 Synthesis of Dipeptide Functionalized Benzo[ghi]perylene Monoimide

In general, the widely followed pathway to synthesis benzo[ghi]perylene monoimide is a Diels-Alder reaction of perylene with maleic anhydride and subsequent condensation reaction<sup>42-45</sup> with primary aliphatic amines.<sup>46-49</sup> Herein, we have considered an alternative method to synthesize benzo[ghi]perylene monoimide to obtain the product with high yield in respect of bulky hindered substitute. The dienophile imide derivative has been synthesized by reaction of maleic anhydride with a dipeptide diphenylalanine. Crucial steps involved in the synthesis the dienophile are (i) the reaction of H<sub>2</sub>N-L-Phe-L-Phe-OMe with maleic anhydride for the formation of *N,N'*-maleyl-L-Phe-L-Phe-OMe and (ii) and subsequent cyclization of *N,N'*-maleyl-L-Phe-L-Phe-OMe to form *N,N'*-maleoyl-L-Phe-L-Phe-OMe using 1 equiv. of ZnCl<sub>2</sub> and 1.5 equiv. of HMDS in benzene solvent.<sup>50-51</sup> Finally, a dipeptide Phe-Phe-OMe appended benzo[ghi]perylene monoimide **1** was obtained using Diels-Alder reaction of perylene with *N,N'*-maleoyl-Phe-Phe-OMe as orange color solid powder with 96% yield. Synthetic methodology of N-dipeptide-functionalized benzo[ghi]perylene-1,2-dicarboxylic monoimide (BPI-FF-OMe **1**) and other derivatives have been shown in the supporting information (Scheme S1). Dipeptide attached with BPI core helps to increase the solubility of compound BPI-FF-OMe in a range of organic solvents, which acts as an alternative of mostly used 'swallow' alkyl chains directly attached to the main perylene or PDI moieties.

### 2.2 Synthesis of Leucine Methyl Ester Functionalized Benzo[ghi]perylene Monoimides

Similarly, BPI-L-OMe **2** was synthesized by (i) the reaction of H<sub>2</sub>N-L-Leu-OMe with maleic anhydride for the formation of *N,N'*-maleyl-L-Leu-OMe **6b** and (ii) and subsequent cyclization of

*N,N'*-maleyl-L-Leu-OMe to form *N,N'*-maleoyl-L-Leu-OMe **7b** using 1 equiv. of ZnCl<sub>2</sub> and 1.5 equiv. of HMDS in benzene solvent.<sup>50-51</sup> Finally, a Leu-OMe appended benzo[ghi]perylene monoimide **2** was obtained using Diels-Alder reaction of perylene with *N,N'*-maleoyl-L-Leu-OMe **7b** as a red solid powder with 76% yield.

### 2.3 Photophysics of Dipeptide Functionalized Benzo[ghi]perylene Monoimide

UV-vis absorption study was performed to determine the optical and electronic properties of synthesized BPI-FF-OMe. UV-vis absorption spectra of BPI-FF-OMe were recorded in various solvents of different polarity (Figure 1A and Figure S1). UV-vis absorption spectra show characteristic absorption bands between 325-500 nm in an aprotic solvent toluene. The strongest absorption peak at 341 nm with molar absorptivity 51000 M<sup>-1</sup>cm<sup>-1</sup> is attributed to  $\pi \rightarrow \pi^*$  transition of benzo[ghi]perylene monoimide system. The lowest energy transition at 483 nm with a shoulder at 455 nm corresponds to S<sub>0</sub>→S<sub>1</sub> transition. The absorbance at 455 nm is attributed to the transition at highest excited vibrational level. The minimal blue shift was observed in the UV-vis absorbance spectra of BPI-FF-OMe when changing the solvent from aprotic non-polar toluene to protic polar solvent methanol (Figure 1A). In general, polar solvents play an important role in stabilization of molecules in ground state and excited state which lead to either hypsochromic or bathochromic shift in the absorption maxima.<sup>52</sup> The  $\lambda_{\text{max}}$  of BPI-FF-OMe in ten different solvents are listed in Table 1.

Later, we tried to evaluate the fluorescence properties of the fluorophore BPI-FF-OMe. The emission of BPI-FF-OMe strongly depends on solvent polarity. Herein, we observed that the effect of solvent polarity on the emission maxima was more pronounced than the absorption maxima (Figure 2A and S2). The emission maxima of BPI-FF-OMe in various aprotic to protic solvents

are listed in Table 1. Excitation wavelength at 337 nm was used to collect the emission spectra of compound BPI-FF-OMe. The emission of BPI-FF-OMe shifts from green emission to yellow emission in the visible region as a function of increasing solvent polarity (Figure 2A). BPI-FF-OMe exhibits emission maxima at 508 nm in aprotic toluene solvent whereas the emission was shifted to 566 nm in polar protic methanol solvent. The strong red shift of about 58 nm was observed with decrease in both the fluorescence intensity as well as the quantum yield (Table 1) upon increase in solvent polarity. The peak broadening was also observed with increase in solvent polarity. The shift in fluorescence maximum was attributed due to the solvent polarizability factors ( $\Delta f$ ) of different solvents. The excited state dipole moment ( $\mu_e$ ) of a molecule is different in toluene and methanol which leads to the variation of change in dipole moment  $\Delta\mu$  ( $\Delta\mu = \mu_e - \mu_g$ ). This dipole moment ( $\Delta\mu$ ) directs the excited state energy levels of a molecule in a solvent.<sup>46</sup> The excited state energy level is lower in methanol than toluene. Therefore, energy gap difference is lower in methanol than toluene and corresponding fluorescence emission is shifted to longer wavelength (red shift). Similarly, BPI-L-OMe is also synthesized to determine the role of dipeptide in emissions. Spectroscopic analysis of BPI-L-OMe exhibits similar emission to BPI-FF-OMe (Figure S3). Thus, benzo[ghi]perylene moiety plays an important role in the emission as well as chromic effects for two synthesized compounds.

The excitation spectrum for the 564 nm emission band of BPI-FF-OMe in methanol solvent shows the peaks at 315 nm, 327 nm, 369 nm, 384 nm, 453 nm and 476 nm which is similar to the absorption spectrum with a 30 nm red shift (Figure S4). The fluorescence quantum yields ( $\phi_{un}$ ) of BPI-FF-OMe in ten different solvents are listed in Table 1. The fluorescence quantum yield of BPI-FF-OMe was found to be in between 0.39 in methanol and 0.55 in toluene. The nature of

solvents plays an important role in emission of BPI-FF-OMe. Similar observation was reflected from the optical images of BPI-FF-OMe in different solvents under UV light at a wavelength of 365 nm. The compound BPI-FF-OMe showed green fluorescence in aprotic non-polar solvent toluene while yellow fluorescence was observed in polar protic methanol solvent (Scheme 1).

A mirror image relationship between the electronic transitions of  $S_0 \rightarrow S_1$  (absorption) and  $S_1 \rightarrow S_0$  (emission) of BPI-FF-OMe in aprotic nonpolar toluene solvent is clearly observed at the wavelength of 410 nm - 590 nm (Figure 2B).<sup>46-47</sup> Solvent dependent Stokes shifts for BPI-FF-OMe was interpreted in terms of the Lippert-Mataga equation. Stokes shifts calculated from lower energy transition of BPI-FF-OMe molecule (Figure 3A). Figure 3B represents the Lippert-Mataga plot of  $S_1 \rightarrow S_0$  Stokes' shift  $\Delta\bar{\nu}$  versus  $\Delta f$  for molecule **1** in the solvents listed in Table 1. The plot depicts a good linear relationship of  $\Delta\bar{\nu}$  and  $\Delta f$ .

Time Correlated Single Photon Counting (TCSPC) experiment was performed to determine the average fluorescence lifetime of BPI-FF-OMe. To measure the average fluorescence decay traces of BPI-FF-OMe, the samples were excited at 376 nm and the emissions were monitored at 508 nm for toluene and 566 nm for methanol. The excited state lifetime ( $\tau$ ) of BPI-FF-OMe decreases with increasing in solvent polarity from 8.4 ns in toluene to 5.7 ns in methanol (Figure 4).

## 2.4 Theoretical Calculation

DFT calculation was performed to determine the energy minimized geometry of BPI-FF-OMe in ground state. Theoretical calculation of highest occupied molecular orbital (HOMO) and lowest unoccupied molecular orbital (LUMO) of synthesized compound BPI-FF-OMe were calculated using the B3LYP/6-31G\* basis set of Gaussian 09 program. The highest occupied molecular

orbital (HOMO) and lowest unoccupied molecular orbital (LUMO) levels of BPI-FF-OMe **1** molecule are -5.57 eV and -2.50 eV respectively. HOMO of the molecule is mostly found on conjugated BPI core and the LUMO mostly exists at imide nitrogen of BPI core (Figure 5). HOMO/LUMO calculation determines the band gap energy of molecules.<sup>53</sup> The calculated band gap energy of BPI-FF-OMe is 3.06 eV. The optical band gap 2.6 eV was calculated from the experiment performed on UV-Visible spectroscopy in methanol. It is found that N-capped dipeptide appended BPI molecule has no effect on the HOMO and LUMO distribution of BPI core.

## 2.5 Self-assembly Study of BPI-FF-OMe

Variable temperature dependent <sup>1</sup>H NMR study was performed in DMSO-d<sub>6</sub> to understand the various non-covalent interactions responsible for the self-assembly nature of aromatic dipeptide Phe-Phe-OMe functionalized benzo[ghi]perylene monoimide (BPI-FF-OMe). The change in chemical shift ( $\delta$ ) of aromatic BPI ring protons and peptide NH proton with different temperatures suggests the presence of intermolecular H-bonding and  $\pi$ - $\pi$  stacking interactions of BPI-FF-OMe molecules. A significant change in chemical shift ( $\delta$ ) was observed for NH proton of dipeptide backbone. The chemical shift of NH proton was shifted to up-field (8.86 ppm to 8.60 ppm) with increase in temperature from 303 K to 343 K (Figure 6). The up-field shifting is due to the weaker H-bonding between BPI molecules and corresponding dis-assembly on warming.<sup>54-57</sup> Moreover, the down-field  $\delta$  shift of BPI protons with increasing temperature is the evidence in favor of  $\pi$ - $\pi$  stacking interactions. <sup>1</sup>H NMR signals of all benzo[ghi]perylene ring protons shifted to down-field because the aromatic ring protons of benzo[ghi]perylene moieties experience de-shielding effect from the ring current at high temperature where the interacting  $\pi$  clouds of aromatic protons are loosely associated to each other than the lower temperature.<sup>58-59</sup>

Therefore, H-bonding and  $\pi$ - $\pi$  stacking interactions play the crucial role in the stabilization of self-assembly structure of BPI-FF-OMe molecule where the amide functionality of peptide backbone provides hydrogen-bonding interaction and benzo[ghi]perylene monoimide protons contributes in  $\pi$ - $\pi$  stacking interactions. The amphiphile BPI-FF-OMe form self-assembled nanospherical structures in different solvents. To further investigate the formation, stability and equilibrium state of nanospheres, the particle size distribution was analyzed by dynamic light scattering (DLS) experiments in methanol and toluene at 25 °C (Figure 7). The hydrodynamic diameters of nanospheres 857 nm and 613 nm were observed in DLS analysis (Table S2). Polydispersity index was calculated as 0.47 in toluene and 0.30 in methanol solutions. These results suggest that nanospheres are polydisperse both in toluene and methanol solutions. The estimated zeta-potential of formed nanospheres of BPI-FF-OMe were -25.89 mV and -17.97 mV in toluene and methanol respectively. These zeta potential determine the surface charge of nanospheres.

## 2.6 Morphological Characterization: Supramolecular Nanospheres

Scanning electron microscope (SEM), transmission electron microscope (TEM) was used to explore the morphology of BPI-FF-OMe in an aprotic solvent toluene and protic solvent methanol. The solution of BPI-FF-OMe in toluene and methanol showed well organized uniform nanosphere architectures (Figures 8A and 8B). The possible mechanism for nanosphere formation could lead via micellar formation in the initial stage followed by higher order self-assembly into the nanosphere architectures (Scheme 2). An aromatic dipeptide Phe-Phe-OMe functionalized benzo[ghi]perylene-monoimide (BPI-FF-OMe) self-organized into nanospheres via intermolecular hydrogen bonding and  $\pi$ - $\pi$  stacking interactions in toluene and methanol. SEM results are consistent with the results obtained from TEM analysis (Figure 8C and 8D).

Atomic force microscopic images were recorded upon drop casting of a solution of BPI-FF-OMe on glass substrate. The AFM images showed the similar characteristics features of nanosphere architectures which were observed for the SEM and TEM analysis. The average heights of nanosphere architectures are 176 nm in methanol and 203 nm in toluene (Figures 9A and 9B). Scheme 2 depicts the possible self-assembly process of BPI-FF-OMe into nanospherical architectures.

## 2.7 Donor-acceptor Interactions Lead to White Light Emission

The aromatic  $\pi$ - $\pi$  stacking interaction of BPI-FF-OMe was utilized in white light emission through the co-assembly with 1-pyrenebutyric acid (PyBA). PyBA was selected because it contains  $\pi$ -conjugated aromatic moiety. Both the aromatic donor and acceptor molecules can participate in aromatic  $\pi$ - $\pi$  stacking interaction and lead to energy transfer. Solution of donor PyBA to acceptor BPI-FF-OMe **1** in methanol show white light emission upon exposure to a UV lamp at 365 nm (Scheme 1).

UV-Vis spectroscopic studies were performed to examine spectral characteristic features of different molar ratios of donor and acceptor molecules (Figure 10A). Emission spectra were also collected to establish the mechanism of energy transfer from donor PyBA to acceptor BPI-FF-OMe **1** molecules. Titrating PyBA with BPI-FF-OMe **1**, emission spectra were recorded at an excitation wavelength of 341 nm. The gradual addition of BPI-FF-OMe **1** to PyBA, a steady decrease in fluorescence intensity at 375 nm, 395 nm, 415 nm and a concomitant increase of a new peak at 568 nm (Figure 10B) was observed. The energy transfer from donor PyBA to acceptor BPI-FF-OMe is well noticeable upon quenching emission peak of donor and subsequently enhancement of emission of acceptor molecules in methanol (Figure 10C). In

general, white light is constituted by many wavelengths. The emission spectra of equimolar mixture of donor PyBA and acceptor BPI-FF-OMe show various emission peaks in the range of 350 nm to 650 nm (Figure S5).

The individual emission of BPI-FF-OMe and PyBA in a protic methanol solvent was analyzed. BPI-FF-OMe emits yellow fluorescence upon exposure to UV lamp at 365 nm. However, a solution of PyBA shows blue emission under UV lamp at 365 nm (Figure 10D). The combination of donor-acceptor pair at different molar ratio shows remarkable changes in the emission. A white light emission was observed when a pair of donor (PyBA)-acceptor (BPI-FF-OMe) (10:1) was exposed to UV lamp at 365 nm in methanol (Figure 9B and D). The white light emission was observed due to the energy transfer between donor and acceptor. The white light emitting solution of PyBA:BPI-FF-OMe coated over the silica plate shows excellent white light emission (Figure S6). Thus, the solution PyBA:BPI-FF-OMe can be used for the coating purpose in various materials. Similarly, BPI-L-OMe also exhibits white light emission upon mixing with different molar ratio of PyBA (Figure S7 and S8) which is confirmed by fluorescence spectroscopy (Figure S8).

### 3. CONCLUSION

In this work, we have synthesized an aromatic benzo[ghi]perylene monoimide capped derivatives BPI-FF-OMe and BPI-L-OMe. The optical behavior of BPI-FF-OMe was studied in a wide range of organic solvents. BPI-FF-OMe preferably forms nanospherical architecture both in protic polar and aprotic solvents like methanol and toluene. Intermolecular hydrogen bonding and aromatic  $\pi$ - $\pi$  stacking interactions play important role in the formation of

nanospherical architecture of dipeptide functionalized benzo[ghi]perylene monoimide (BPI-FF-OMe). Temperature dependent  $^1\text{H-NMR}$  studies support the intermolecular interactions in solution phase self-assembly of BPI-FF-OMe. The microscopic techniques including SEM, TEM and AFM elucidate the nanostructural morphology of BPI-FF-OMe. The theoretical studies also support the experimental results. The acceptor benzo[ghi]perylene monoimide BPI-L-OMe molecule also shows white light emission through efficient energy transfer between donor acceptor pairs where pyrenebutyric acid was used as an efficient donor molecule. These results could be an efficient approach for the construction of new organic light emitting devices.

## 4. EXPERIMENTAL SECTION

### 4.1 Materials

All reagents and solvents were purchased from commercial sources and used without purification. Solvents were distilled from appropriate drying agents prior to use.<sup>60</sup> Milli-Q water was used whenever was required.

### 4.2 General characterization

All NMR characterizations were carried out on a Bruker AV 400 MHz spectrometer at 300 K. Compound concentrations were in the range 5-10 mmol L<sup>-1</sup> in CDCl<sub>3</sub> and (CD<sub>3</sub>)<sub>2</sub>SO. Mass spectra were recorded on a Bruker micrOTOF-Q II by positive mode electrospray ionisation. Dynamic light scattering (DLS) and zeta potential measurements were made with a NanoPlus-3 zeta/nano particle analyzer (Micromeritics Instrument). The errors for  $d_h$  and  $\xi$  values were  $\pm 2$  nm and  $\pm 10\%$ , respectively. Field Emission Scanning Electron Micrographs (FE-SEM) were recorded in a Carl Zeiss supra 55 operated at an accelerating voltage 200 kV. For SEM study, BPI-FF-OMe (6 mmol L<sup>-1</sup>) solutions were dried on a glass slide from respective solvents toluene

and methanol and coated with gold. TEM measurements were performed on a PHILIPS electron microscope (model: CM 200), operated at 200 kV. Samples were prepared by placing a drop of the solution on carbon coated copper grids and dried under lamp. AFM measurements were performed on a scanning probe microscope AIST-NT instrument (model no. smartSPM-1000). The samples were prepared by drop casting on glass substrate and dried under vacuum.

Compound **1** was dissolved in respective solvents. The samples were allowed to stand for 48 hours at room temperature. Then the solutions drop casted on to the glass substrate and allow to dry for scanning electron microscopic study.

UV-Vis absorption spectra of samples were recorded using a Varian Cary100 Bio UV-Vis spectrophotometer.

Fluorescence spectra of samples were recorded on a Horiba Scientific Fluoromax-4 spectrophotometer with a 1 cm path length quartz cell at room temperature. The slit width for the excitation and emission was set at 2 nm and 1 nm data pitch. Excitations of samples were performed at 338 nm and the data range was in between 348 to 666 nm.

The fluorescence quantum yields in various solvents were calculated using steady-state comparative method using fluorescein as a standard ( $\phi_{std} = 0.79$ ).<sup>61-62</sup>

$$\phi_{un} = \phi_{std} \times \frac{S_{un}}{S_{std}} \times \frac{A_{std}}{A_{un}} \times \frac{n^2 D_{un}}{n^2 D_{std}} \quad (1)$$

$\phi_{un}$  is the quantum yield of the unknown sample and  $\phi_{std}$  is the emission quantum yield of the standard compound.  $A_{std}$  and  $A_{un}$  represent the absorbance of the standard and the sample at the excitation wavelength, while  $S_{std}$  and  $S_{un}$  are the integrated emission band areas of the standard and the sample respectively.  $nD_{std}$  and  $nD_{un}$  are the solvent refractive index of the standard and

the sample respectively. Here, “un” stands for unknown sample and “std” stands for standard sample. The values are quite similar to the previously studied structurally similar fluorophores.<sup>63</sup> Time resolved studies were performed using a time correlated single photon counting (TCSPC) system from Horiba Yovin (Model: Fluorocube-01-NL). Samples were excited at 376 nm using a picosecond diode laser (Model: Pico Brite-375L).

The amplitude-weighted lifetime is estimated by

$$\langle \tau \rangle = \sum_{i=1}^n a_i \tau_i \quad (4)$$

where  $\tau_i$  are the fluorescence lifetime of various fluorescent species,  $a_i$  are the normalized pre-exponential factors. The goodness of the fit is judged by the reduced chi-square ( $\chi^2$ ) value.

## 2.1 Synthesis of BPI-FF-OMe

H<sub>2</sub>N-L-Phe-L-Phe-OMe **5** was synthesized according to the literature through intermediates **3** and **4**.<sup>64</sup> 1.63 g (5 mmol) of H<sub>2</sub>N-L-Phe-L-Phe-OMe **6** was taken in 8 mL ethyl acetate. Maleic anhydride (0.735 g, 7.5 mmol) was dissolved into the ethyl acetate and added to the reaction mixture at room temperature. After stirred over 24 h, the mixture was fully washed with H<sub>2</sub>O, saturated brine and dried over Na<sub>2</sub>SO<sub>4</sub>. The above solution was concentrated by rotary evaporator to obtain the product *N*-maleyl-L-Phe-L-Phe-OMe **6a** as white powder. 1.50 g (3.5 mmol) of *N*-maleyl-L-Phe-L-Phe-OMe **6a** was dissolved in benzene and put into a double-neck flask. The solution was heated to 50 °C and 0.48 g (3.5 mmol) ZnCl<sub>2</sub> was added. Then, the solution of 0.85 g (5.25 mmol) 1,1,1,3,3,3-hexamethyldisilazane (HMDS) in benzene was added drop wise into the reaction mixture at 80 °C, and kept 12 h with stirring. Then, the mixture was

poured into 600 mL 0.5 (N) HCl and stirred until clear solution was obtained. The organic layer was separated, the aqueous phase was extracted with 300 mL EtOAc. The combined organic layer was washed with 3×100 mL NaHCO<sub>3</sub> and brine solution and dried over Na<sub>2</sub>SO<sub>4</sub>. The organic layer was evaporated under vacuum to obtain the product *N*-maleoyl-L-Phe-L-Phe-OMe **7a**. Perylene (0.504 g, 2 mmol), *N*-maleoyl-L-Phe-L-Phe-OMe **7a** (1.2192 g, 3 mmol) and chloranil (1.0326 g, 4.2 mmol) were thoroughly mixed and heated at 240 °C with stirring for 3 h. The mixture solidified after cooling at room temperature. Chloroform was added to dissolve the solidified mass. The mixture was purified using a silica gel column with chloroform/ether (1:1) as eluent. The compound benzo[ghi]perylene-1,2-dicarboxylic(L-Phe-L-Phe-OMe)imide **1** was collected as orange solid.

*N*-maleyl-L-Phe(1)-L-Phe(2)-OMe **6a**: Yield 3.0 g (7.07 mmol, 94.33%) <sup>1</sup>H NMR (400 MHz, DMSO-d<sub>6</sub>): δ = 9.65 (d, 1H, *J* = 8.82 Hz), 9.09 (d, 1H, *J* = 7.76 Hz), 7.60-7.69 (m, 10H, aromatic protons), 6.76 (d, 1H, *J* = 12.52 Hz), 6.66 (d, 1H, *J* = 12.56 Hz), 5.05 (m, 1H, C<sup>α</sup>H of Phe(2)), 4.91 (m, 1H, C<sup>α</sup>H of Phe(1)), 3.99 (s, 3H, -OCH<sub>3</sub>), 3.44 (m, 2H, C<sup>β</sup>Hs of Phe), 3.35 (m, 1H, C<sup>β</sup>H of Phe), 3.16 (m, 1H, C<sup>β</sup>H of Phe). MS (ESI) *m/z* for C<sub>23</sub>H<sub>24</sub>N<sub>2</sub>O<sub>6</sub>Na (M+Na)<sup>+</sup> calcd.: 447.1532, found: 447.1577.

*N*-maleoyl-L-Phe(1)-L-Phe(2)-OMe **7a**: Yield = 1.3912 g (3.42 mmol, 96.86%). <sup>1</sup>H NMR (400 MHz, CDCl<sub>3</sub>): δ = 6.98-7.21 (m, 10H, aromatic protons), 6.48 (s, 2H), 6.35 (d, 1H, *J* = 7.24 Hz, NH), 4.76-4.82 (m, 2H, C<sup>α</sup>Hs of Phe(1) and Phe(2)), 3.65 (s, 3H, -OMe), 3.28-3.30 (m, 2H, C<sup>β</sup>Hs), 3.07-3.12 (m, 1H, C<sup>β</sup>H), 2.97-3.02 (m, 1H, C<sup>β</sup>H). MS (ESI) *m/z* for C<sub>23</sub>H<sub>22</sub>N<sub>2</sub>O<sub>5</sub>Na (M+Na)<sup>+</sup> calcd.: 429.1426, found: 429.1470.

Benzo[ghi]perylene-1,2-dicarboxylic(L-Phe-L-Phe-OMe)imide **1**: Yield = 1.26 g (1.93 mmol, 96.92%).  $^1\text{H}$  NMR (400 MHz,  $\text{CDCl}_3$ )  $\delta$  = 8.60 (d, 2H,  $J$  = 8Hz ), 8.39 (d, 2H,  $J$  = 8Hz), 7.65-7.73 (m, 6H), 7.23 (d, 2H,  $J$  = 8 Hz), 7.04 (d, 2H,  $J$  = 4 Hz), 7.12 (t, 2H), 7.01 (t, 2H), 6.93 (t, 2H), 6.85 (d, 1H, NH ), 5.28 (m, 1H,  $\text{C}^\alpha\text{H}$  of Phe(1)), 4.97 (m, 1H,  $\text{C}^\alpha\text{H}$  of Phe(2)), 3.68 (s, 3H, -OCH<sub>3</sub>), 3.23 (d,  $\text{C}^\beta\text{H}$  of Phe(1)), 3.18 (d,  $\text{C}^\beta\text{H}$  of Phe(1)), 3.07 (d,  $\text{C}^\beta\text{H}$  of Phe(2)), 3.03 (d,  $\text{C}^\beta\text{H}$  of Phe(2)). MS (ESI)  $m/z$  for  $\text{C}_{43}\text{H}_{30}\text{N}_2\text{O}_5\text{Na}$  ( $\text{M}+\text{Na}$ )<sup>+</sup> calcd.: 677.2052, found: 677.2096.

Maleyl-L-Leu-OMe **6b**: Yield 0.78 g (3.46 mmol, 98.99%)  $^1\text{H}$  NMR (400 MHz, DMSO  $d_6$ ):  $\delta$  = 13.76 (s, 1H), 9.06 (d, 1H, -NH-), 6.35 (d, 1H), 6.28 (d, 1H) 4.36 (m, 1H,  $\text{C}^\alpha\text{H}$  of Leu), 3.63 (s, 3H), 1.57 (m, 2H,  $\text{C}^\beta\text{H}$  of Leu), 1.19 (m, 1H,  $\text{C}^\gamma\text{H}$  of Leu), 0.88 (d, 3H,  $\text{C}^\delta\text{H}$  of Leu,  $J$  = 6.24 Hz), 0.85 (d, 3H,  $\text{C}^\delta\text{H}$  of Leu,  $J$  = 6.28 Hz).

Maleoyl-L-Leu-OMe **7b**: Yield 1.62 g (6.65 mmol, 90.07%)  $^1\text{H}$  NMR (400 MHz,  $\text{CDCl}_3$ ):  $\delta$  = 6.74 (s, 2 H), 4.75 (m, 1H,  $\text{C}^\alpha\text{H}$  of Leu), 3.72 (s, 3H), 2.23 (m, 1H,  $\text{C}^\beta\text{H}$  of Leu), 1.87 (m, 1H,  $\text{C}^\beta\text{H}$  of Leu), 1.14 (m, 1H,  $\text{C}^\gamma\text{H}$  of Leu), 0.92 (d, 3H,  $\text{C}^\delta\text{H}$  of Leu,  $J$  = 3.24 Hz), 0.90 (d, 3H,  $\text{C}^\delta\text{H}$  of Leu,  $J$  = 3 Hz).

Benzo[ghi]perylene-1,2-dicarboxylic(L-Leu-OMe)imide **2**: Yield = 0.7259g (1.99 mmol, 76.74%).  $^1\text{H}$  NMR (400 MHz,  $\text{CDCl}_3$ ):  $\delta$  = 9.14 (d, 2 H,  $J$  = 9.04Hz), 8.98 (d, 2H,  $J$  = 7.76 Hz), 8.19 (d, 2H,  $J$  = 7.8 Hz), 8.15 (d, 2H,  $J$  = 9Hz), 8.08 (t, 2H), 5.18 (m, 1H,  $\text{C}^\alpha\text{H}$  of Leu), 3.84 (s, 3H), 2.52 (m, 1H,  $\text{C}^\beta\text{H}$  of Leu), 2.13 (m, 1H,  $\text{C}^\beta\text{H}$  of Leu), 1.72 (m, 1H,  $\text{C}^\gamma\text{H}$  of Leu), 1.08 (d, 3H,  $\text{C}^\delta\text{H}$  of Leu,  $J$  = 6.52 Hz ), 1.02 (d, 3H,  $\text{C}^\delta\text{H}$  of Leu,  $J$  = 6.8 Hz).

#### ACKNOWLEDGMENTS

This work was partially supported by Council of Scientific and Industrial Research (CSIR) Project No. 02(0056)/12/EMR-II. We thank SAIF, IITB for the assistance of EM facility.

**Supporting information:** Optical images, spectroscopic data, NMR and Mass data.

## REFERENCES

- 1 F. Würthner, A. Sautter, C. Thalacker, *Angew. Chem. Int. Ed.*, 2000, **39**, 1243-1245.
- 2 L. Zang, Y. Che, J. S. Moore, *Acc. Chem. Res.*, 2008, **41**, 1596-1608.
- 3 J. D. Tovar, *Acc. Chem. Res.*, 2013, **46**, 1527-1537.
- 4 A. P. H. J. Schenning, E. W. Meijer, *Chem. Commun.*, 2005, 3245-3258.
- 5 F. J. M. Hoeben, P. Jonkheijm, E. W. Meijer, A. P. H. J. Schenning, *Chem. Rev.*, 2005, **105**, 1491-1546.
- 6 J. Ide, R. Mereau, L. Ducasse, F. Castet, *J. Phys. Chem., B* 2011, **115**, 5593-5603.
- 7 Y. Avlasevich, C. Li, K. Mullen, *J. Mater. Chem.*, 2010, **20**, 3814-3826.
- 8 H. Langhals, S. Kirner, *Eur. J. Org. Chem.*, 2000, 365-380.
- 9 Y. Zagranyarski, L. Chen, D. Jänsch, T. Gessner, C. Li, K. Müllen, *Org. Lett.*, 2014, **16**, 2814-2817.
- 10 A. Jana, K. T. Nguyen, X. Li, P. Zhu, N. S. Tan, H. Ågren, Y. Zhao, *ACS Nano* 2014, **8**, 5939-5952.
- 11 F. Würthner, *Chem. Commun.*, 2004, 1564-1579.
- 12 S. Vajiravelu, L. Ramunas, G. J. Vidas, G. Valentas, J. Vygintas, Valiyaveetil, S. J. *Mater. Chem.*, 2009, **19**, 4268-4275.
- 13 N. Mizoshita, T. Tani, H. Shinokubo, S. Inagaki, *Angew. Chem., Int. Ed.*, 2012, **51**, 1156-1160.
- 14 J. L. Segura, H. Herrera, P. Bauerle, *J. Mater. Chem.*, 2012, **22**, 8717-8733.
- 15 W. Jeong, S. Choi, J. S. Choi, Y.-B. Lim, *ACS Nano* 2013, **7**, 6850-6857.
- 16 S. Fleming, R. V. Ulijn, *Chem. Soc. Rev.*, 2014, **43**, 8150-8177.
- 17 M. D. Segarra-Maset, V. J. Nebot, J. F. Miravet, B. Escuder, *Chem. Soc. Rev.*, 2013, **42**, 7086-7098.
- 18 Z. Yang, G. Liang, B. Xu, *Acc. Chem. Res.*, 2008, **41**, 315-326.
- 19 E. R. Draper, J. J. Walsh, T. O. McDonald, M. A. Zwijnenburg, P. J. Cameron, A. J. Cowan, D. J. Adams, *J. Mater. Chem. C* 2014, **2**, 5570-5575.

- 20 Y. Che, A. Datar, K. Balakrishnan, L. Zang, *J. Am. Chem. Soc.* 2007, **129**, 7234-7235.
- 21 K. Balakrishnan, A. Datar, R. Oitker, H. Chen, J. Zuo, L. Zang, *J. Am. Chem., Soc.* 2005, **127**, 10496-10497.
- 22 K. Balakrishnan, A. Datar, T. Naddo, J. Huang, R. Oitker, M. Yen, J. Zhao, L. Zang, *J. Am. Chem. Soc.*, 2006, **128**, 7390-7398.
- 23 L. Zhong, F. Xing, W. Shi, L. Yan, L. Xie, S. Zhu, *ACS Appl. Mater. Interfaces* 2013, **5**, 3401-3407.
- 24 X. Feng, Y. An, Z. Yao, C. Li, G. Shi, *ACS Appl. Mater. Interfaces* 2012, **4**, 614-618.
- 25 S. Roy, D. K. Maiti, S. Panigrahi, D. Basak, A. Banerjee, *RSC Adv.*, 2012, **2**, 11053-11060.
- 26 S. Bai, S. Debnath, N. Javid, P. W. J. M. Frederix, S. Fleming, C. Pappas, R. V. Ulijn, *Langmuir* 2014, **30**, 7576-7584.
- 27 G. L. Eakins, J. K. Gallaher, R. A. Keyzers, A. Falber, J. E. A. Webb, A. Laos, Y. Tidhar, H. Weissman, B. Rybtchinski, P. Thordarson, J. M. Hodgkiss, *J. Phys. Chem. B* 2014, **118**, 8642-865.
- 28 B. D. Briggs, M. R. Knecht, *J. Phys. Chem. Lett.*, 2012, **3**, 405-418.
- 29 X. Yan, Y. Cui, Q. He, K. Wang, J. Li, *Chem. Mater.*, 2008, **20**, 1522-1526.
- 30 N. Na, X. Mu, Q. Liu, J. Wen, F. Wang, J. Ouyang, *Chem. Commun.*, 2013, **49**, 10076-10078.
- 31 E. Gazit, *Chem. Soc. Rev.*, 2007, **36**, 1263-1269.
- 32 Z. Gan, X. Wu, X. Zhu, J. Shen, *Angew. Chem. Int. Ed.*, 2013, **52**, 2055-2059.
- 33 R. Abbel, R. Weegen, W. Pisula, M. Surin, P. Leclere, R. Lazzaroni, E. W. Meijer, A. P. H. J. Schenning, *Chem. Eur. J.* 2009, **15**, 9737- 9746.
- 34 C. Vijayakumar, V. K. Praveen, A. Ajayaghosh, *Adv. Mater.*, 2009, **21**, 2059-2063.
- 35 R. Abbel, C. Grenier, M. J. Pouderoijen, J. W. Stouwdam, P. E. L. G. Leclere, R. P. Sijbesma, E.W. Meijer, A. P. H. J. Schenning, *J. Am. Chem. Soc.* 2009, **131**, 833-843.
- 36 F. Liu, C. Tang, Q.-Q. Chen, F.-F. Shi, H.-B. Wu, L.-H. Xie, B. Peng, W. Wei, Y. Cao, W. Huang, *J. Phys. Chem. C*, 2009, **113**, 4641-4647.
- 37 C. Chen, X.-H. Jin, X.-J. Zhou, L.-X. Cai, Y.-J. Zhang, J. Zhang, *J. Mater. Chem. C*, 2015, **3**, 4563-4569.

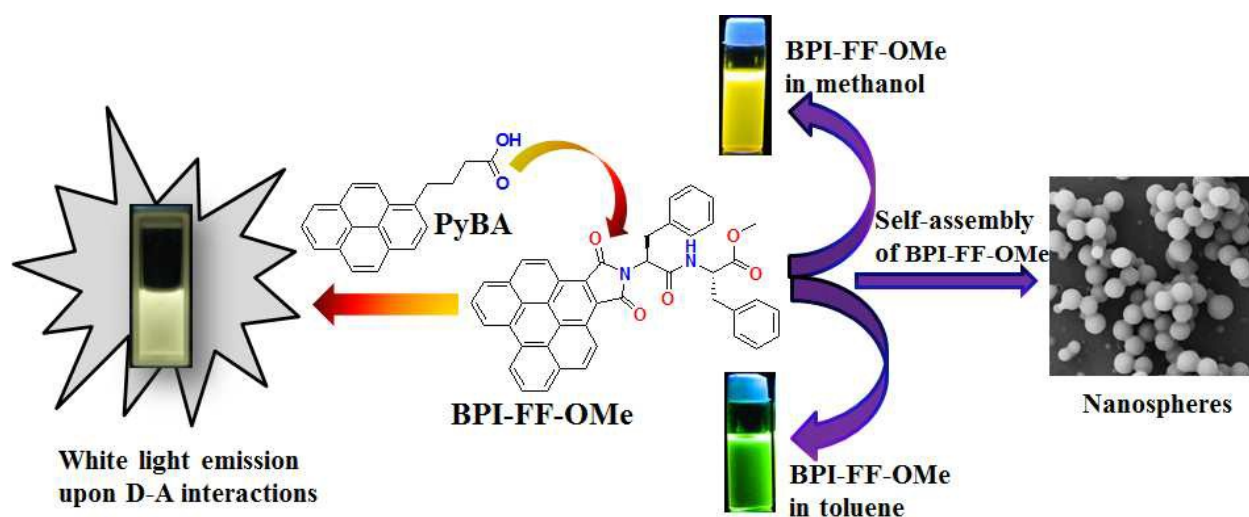
- 38 X.-H. Jin, C. Chen, C.-X. Ren, L.-X. Cai, J. Zhang, *Chem. Commun.*, 2014, **50**, 15878-15881
- 39 I. O. Huyal, U. Koldemir, T. Ozel, H. V. Demir and D. Tuncel, *J. Mater. Chem.*, 2008, **18**, 3568.
- 40 J. Liu, X. Guo, L. Bu, Z. Xie, Y. Cheng, Y. Geng, L. Wang, X. Jing and F. Wang, *Adv. Funct. Mater.*, 2007, **17**, 1917.
- 41 C. Giansante, G. Raffy, C. Schäfer, H. Rahma, M.-T. Kao, A. G. L. Olive, and A. D. Guerzo, *J. Am. Chem. Soc.*, 2011, **133**, 316.
- 42 H. Langhals, B. Bçck, T. Schmid, A. Marchuk, *Chem. Eur. J.*, 2012, **18**, 13188-13194.
- 43 H. Langhals, S. Poxleitner, O. Krotz, T. Pust, *Eur. J. Org. Chem.* **2008**, 4559-4562.
- 44 H. Langhals, M. Speckbacher, *Eur. J. Org. Chem.*, 2001, 2481-2485.
- 45 E. Clar, M. Zander, *J. Chem. Soc.*, **1957**, 4616-4619.
- 46 R S. J. Manning, W. Bogen, L. A. Kellyference, *J. Org. Chem.*, 2011, **76**, 6007-6013.
- 47 K. V. Rao, S. J. George, *Org. Lett.*, 2010, **12**, 2656-2659.
- 48 S. Alibert-Fouet, I. Seguy, J.-F. Bobo, P. Destruel, H. Bock, *Chem. Eur. J.*, 2007, **13**, 1746-1753.
- 49 H. Langhals, *Heterocycles* 1995, **40**, 477-500.
- 50 P. Y. Reddy, S. Kondo, T. Toru, Y. Ueno, *J. Org. Chem.*, 1997, **62**, 2652-2654.
- 51 T. Oishi, H. Gao, T. Nakamura, Y. Isobe, K. Onimura, *Polym. J.*, 2007, **39**, 1047-1059.
- 52 S. S. Bag, M. K. Pradhan, R. Kundu, S. Jana, *Bioorg. Med. Chem. Lett.*, 2013, **23**, 96-101.
- 53 Z. Zhang, H. Huang, X. Yang, L. Zang, *J. Phys. Chem. Lett.*, 2011, **2**, 2897-2905.
- 54 A. Syamakumari, A. P. H. J. Schenning, E. W. Meijer, *Chem. Eur. J.*, 2002, **8**, 3353-3361.
- 55 H. Yu, Y. Lu, X. Chen, K. Liu, Y. Fang, *Soft Matter* 2014, **10**, 9159-9166.
- 56 F. Allix, P. Curcio, Q. N. Pham, G. Pickaert, Jamart-Gregoire B. *Langmuir* 2010, **26**, 16818-16827.
- 57 S. Debnath, A. Shome, S. Dutta, P. K. Das, *Chem. Eur. J.*, 2008, **14**, 6870-6881.
- 58 A. Jain, K. V. Rao, C. Kulkarni, A. George, S. J. George, *Chem. Commun.*, 2012, **48**, 1467-1469.

- 59 L. Brunsveld, H. Zhang, M. Glasbeek, J. A. J. M. Vekemans, E. W. Meijer, *J. Am. Chem. Soc.*, 2000, **122**, 6175-6182.
- 60 D. D. Perrin, W. L. F. Armarego, D. R. Perrin, *Oxford, Pergamon*, 1980.
- 61 J. Q. Umberger, V. K. LaMer, *J. Am. Chem. Soc.*, 1945, **67**, 1099-1109.
- 62 E. Kim, M. Koh, B. J. Lim, S. B. Park, *J. Am. Chem. Soc.*, 2011, **133**, 6642-6649.
- 63 R. Schmidt, J. H. Oh, Y.-S. Sun, M. Deppisch, A.-M. Krause, K. Radacki, H. Braunschweig, M. Konemann, P. Erk, Z. Bao, F. Wurthner, *J. Am. Chem. Soc.*, 2009, **131**, 6215-6228.
- 64 D. B. Rasale, I. Maity, A. K. Das, *RSC Adv.*, 2012, **2**, 9791-9794.

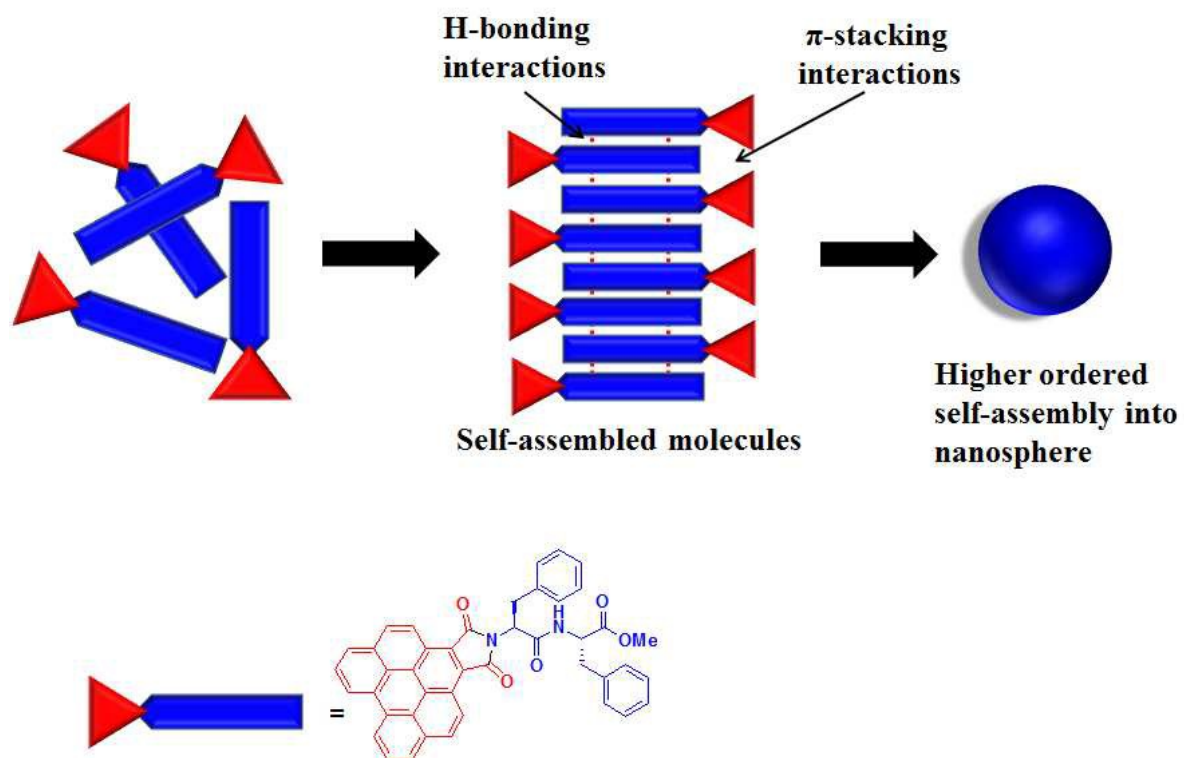
**Table 1.** Spectroscopic and photophysical properties of BPI-FF-OMe in different solvents of increasing polarity.

S. No.	Solvent	$\lambda_{\text{abs}}$ (nm)	$\epsilon_{\text{max}}$ ( $\text{M}^{-1} \text{cm}^{-1}$ )	$\lambda_{\text{em}}$ (nm) <sup>a</sup>	$\Delta\bar{\nu}$ ( $\text{cm}^{-1}$ ) <sup>b</sup>	$\Delta f$	$\tau(\text{ns})$	$\phi_f^c$
1	Toluene	341/391/484	51000	508	976	0.013	8.4	0.55
2	<i>o</i> -xylene	341/391/483	53750	508	1018	0.029	8.4	0.51
3	Benzene	341/390/483	52500	508	1018	0.001	7.5	0.56
4	Tetrahydrofuran	337/389/475	80875	517	1710	0.209	7.9	0.43
5	Chloroform	341/390/487	53125	528	1594	0.149	6.0	0.42
6	Dimethylformamide	338/390/479	50875	535	2185	0.274	7.4	0.51
7	Dimethyl sulfoxide	340/391/480	72875	540	2314	0.263	7.2	0.43
8	Acetonitrile	337/387/479	63000	543	2460	0.305	6.7	0.39
9	Ethanol	337/387/477	47500	557	3011	0.288	6.2	0.38
10	Methanol	337/386/476	42500	566	3340	0.309	5.7	0.39

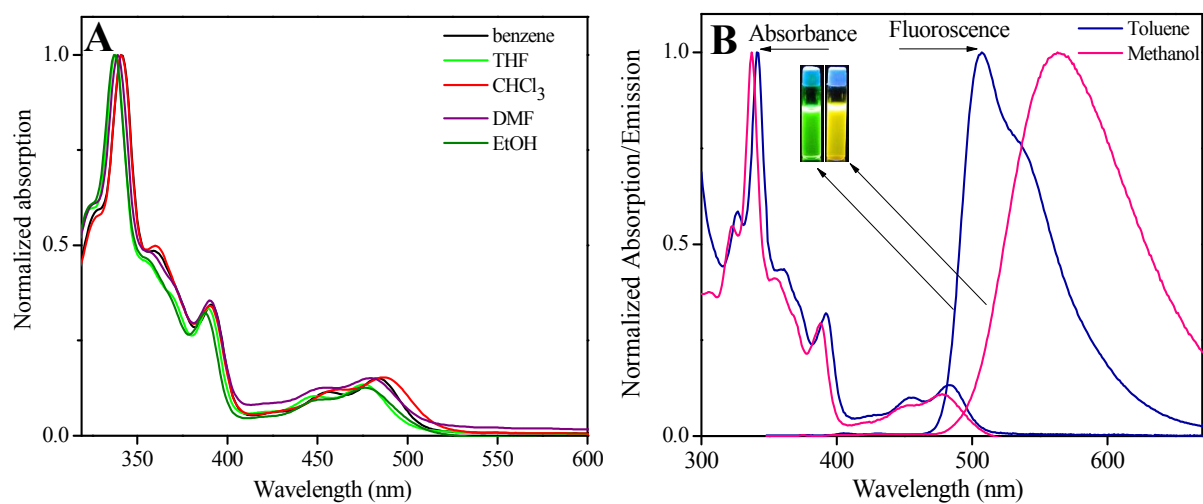
<sup>a</sup>Emission data obtained at  $\lambda_{\text{max}}$  for each solvent. <sup>b</sup>Stokes shift was calculated based on the absorption at lower energy. <sup>c</sup>Quantum yields measured using fluorescein standard in 0.1 (N) NaOH.



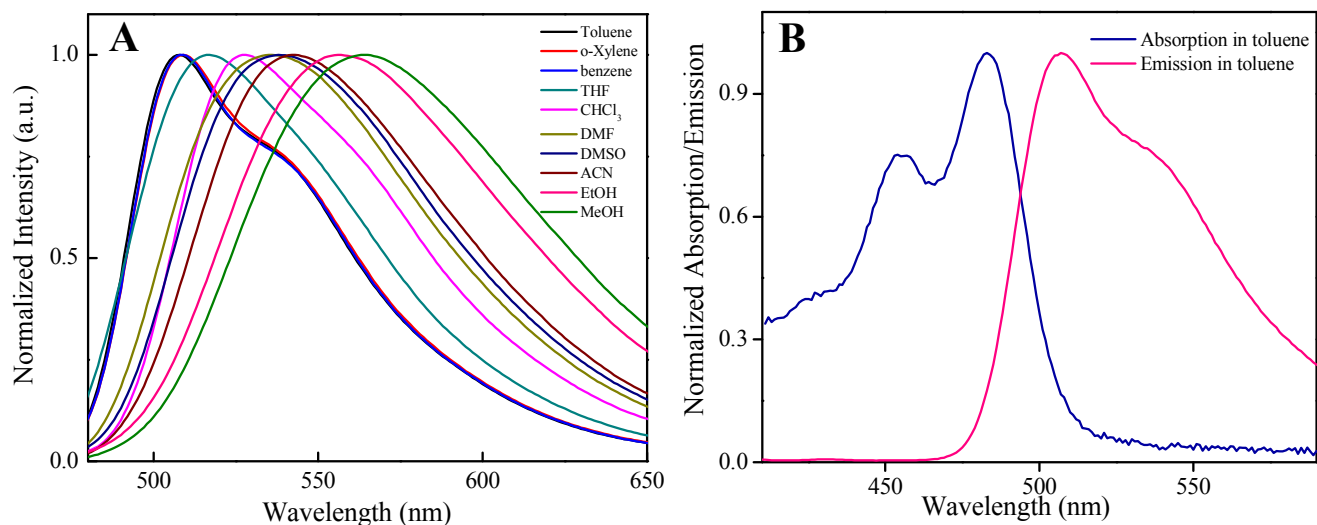
**Scheme 1.** Schematic demonstration represents white light emission upon energy transfer between donor and acceptor (PyBA : BPI-FF-OMe). BPI-FF-OMe molecules shows efficient solvatochromic effects in protic polar solvent methanol and aprotic solvent toluene. BPI-FF-OMe self-assembled to form spherical nanosphere in solution phase.



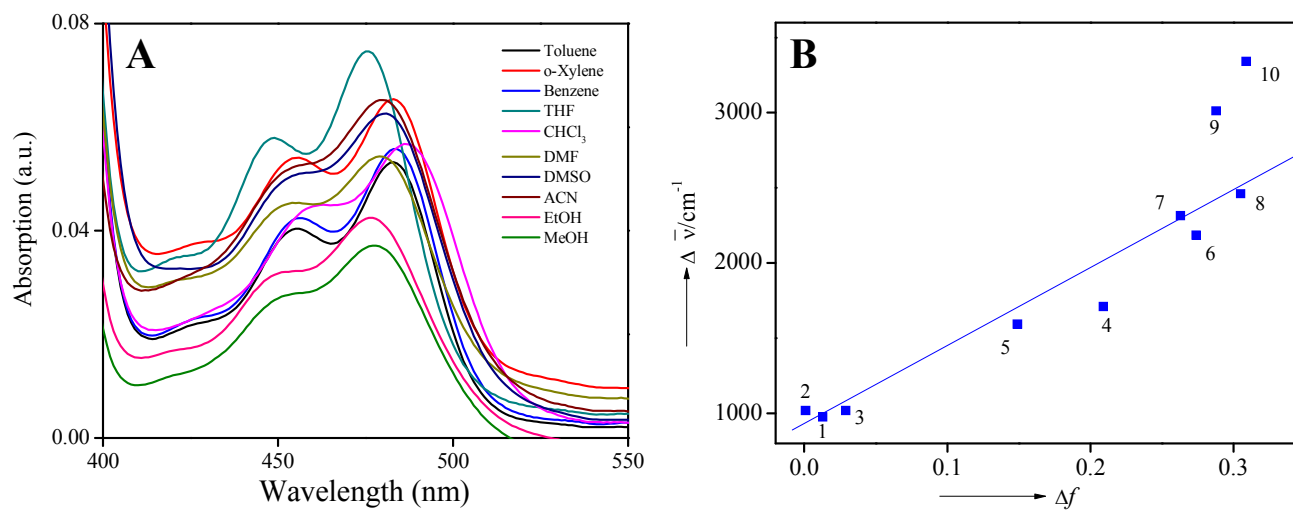
**Scheme 2.** Schematic presentation shows a possible mechanism of BPI-FF-OMe for nanosphere formation.



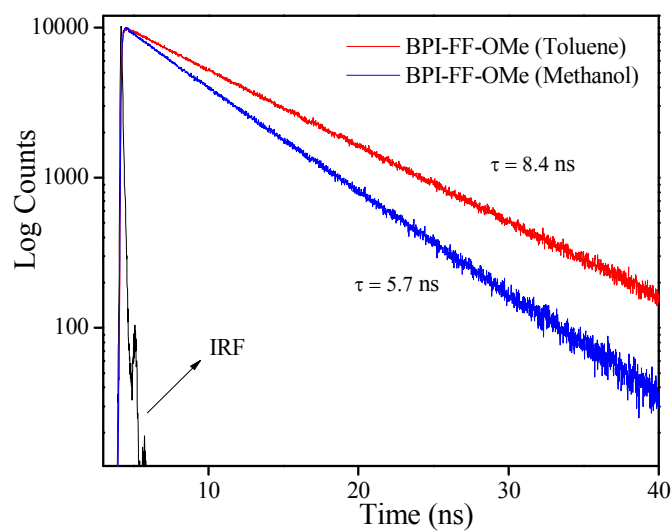
**Figure 1.** (A) Normalized UV-Vis absorption spectra of BPI-FF-OMe ( $8 \times 10^{-6}$  mol L<sup>-1</sup>) in various solvents. (B) Normalized UV-Vis absorption and fluorescence spectra in a non polar solvent toluene (blue) and polar solvent methanol (red). Optical images of BPI-FF-OMe show (green emission in toluene and yellow emission in methanol under 365 nm UV light).



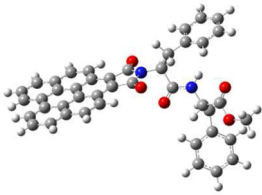
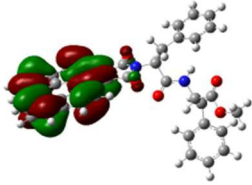
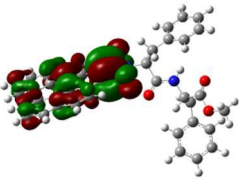
**Figure 2.** (A) Normalized fluorescence spectra of BPI-FF-OME in various non polar to polar solvents listed in Table 1. (B) Fluorescence emission spectra of BPI-FF-OME in toluene normalized with respect to absorption peak at 483 nm.



**Figure 3.** (A) UV-Vis absorption spectra of BPI-FF-OMe in different solvents from listed Table 1 (B) Lippart-Mataga plot: Stokes shift  $\Delta \bar{\nu}$  of BPI-FF-OMe versus Lippart solvent polarizability parameter  $\Delta f$ . The number refers to the solvents in the Table 1. The straight line represents the best linear fit to the 10 data points.



**Figure 4.** Time correlated single photon counting decay traces of BPI-FF-OMe ( $9 \times 10^{-5}$  mol L<sup>-1</sup>) in toluene  $\lambda_{\text{em}} = 508$  nm (red) and methanol  $\lambda_{\text{em}} = 566$  nm (blue).

BPI-FF-OMe	HOMO	LUMO	Calculated Band gap (eV)	Optical band gap(eV) <sup>a</sup>
	 -5.57 eV	 -2.50 eV	3.06 eV	2.6 eV

**Figure 5.** HOMO and LUMO frontier orbital of BPI-FF-OMe at the B3LYP/6-31G (d) level.  
<sup>[a]</sup>Optical band gap of BPI-FF-OMe in methanol was calculated from UV-Vis spectroscopy.

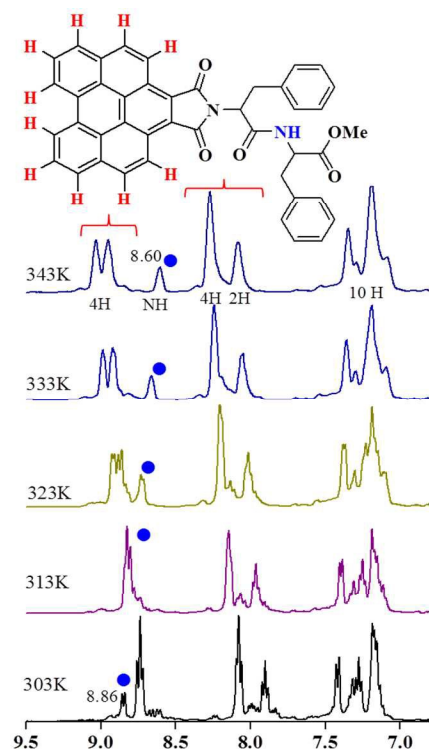


**Figure 6.** Temperature dependent  $^1\text{H}$  NMR spectra of BPI-FF-OMe ( $20 \text{ mmol L}^{-1}$ ) in DMSO- $d_6$ .

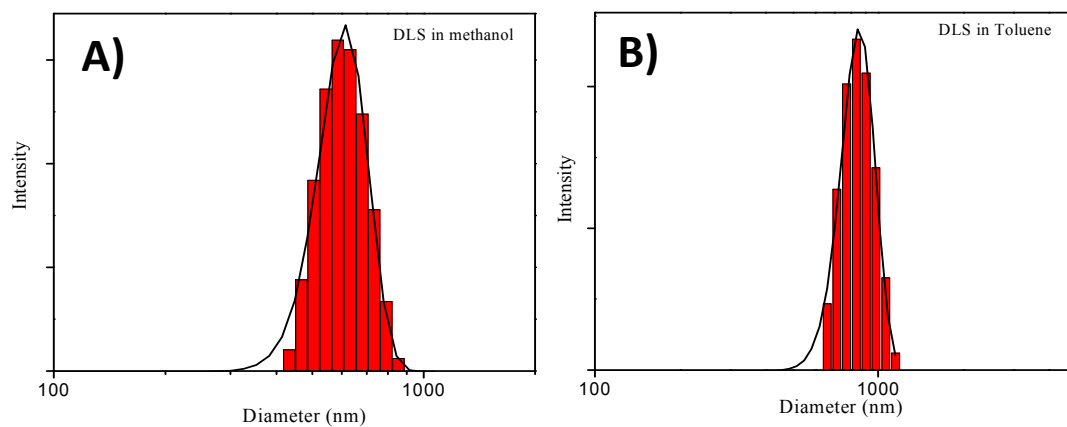


**Figure 7.** Size distribution histogram of nanospheres from DLS measurement. The mean hydrodynamic diameter of nanospheres in (A) methanol and (B) toluene.

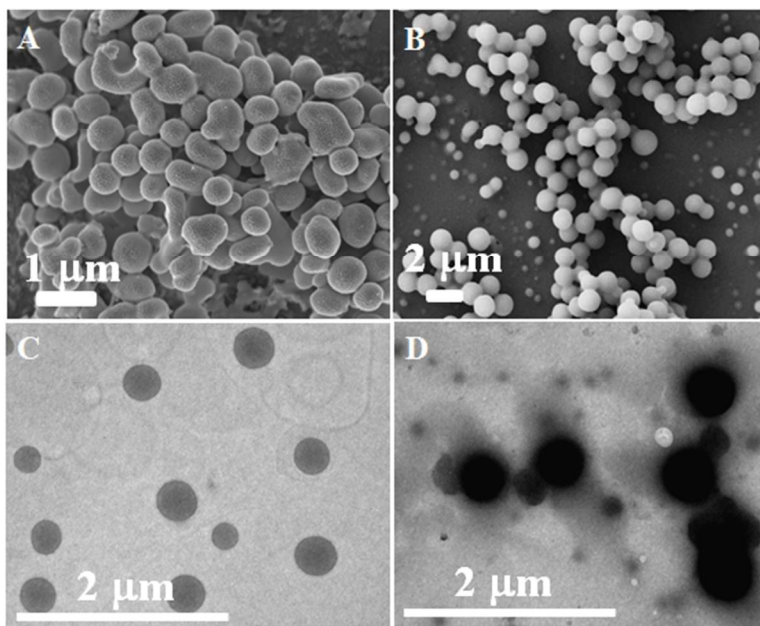


**Figure 8.** Electron microscopic images of BPI-FF-OMe ( $6 \text{ mmol L}^{-1}$ ). (A) SEM image of BPI-FF-OMe in toluene, (B) SEM image of BPI-FF-OMe in methanol, (C) TEM image of BPI-FF-OMe in toluene and (D) TEM image of BPI-FF-OMe in methanol show nanospheres.

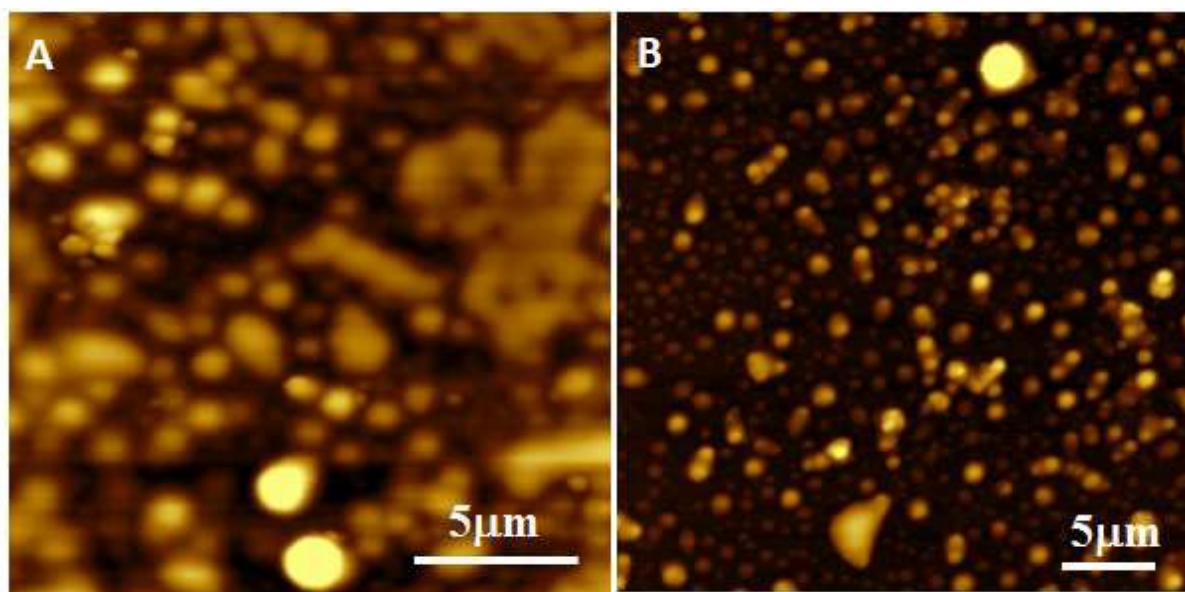


**Figure 9.** AFM images show the nanospherical morphology of BPI-FF-OMe (A) in toluene and (B) in methanol.

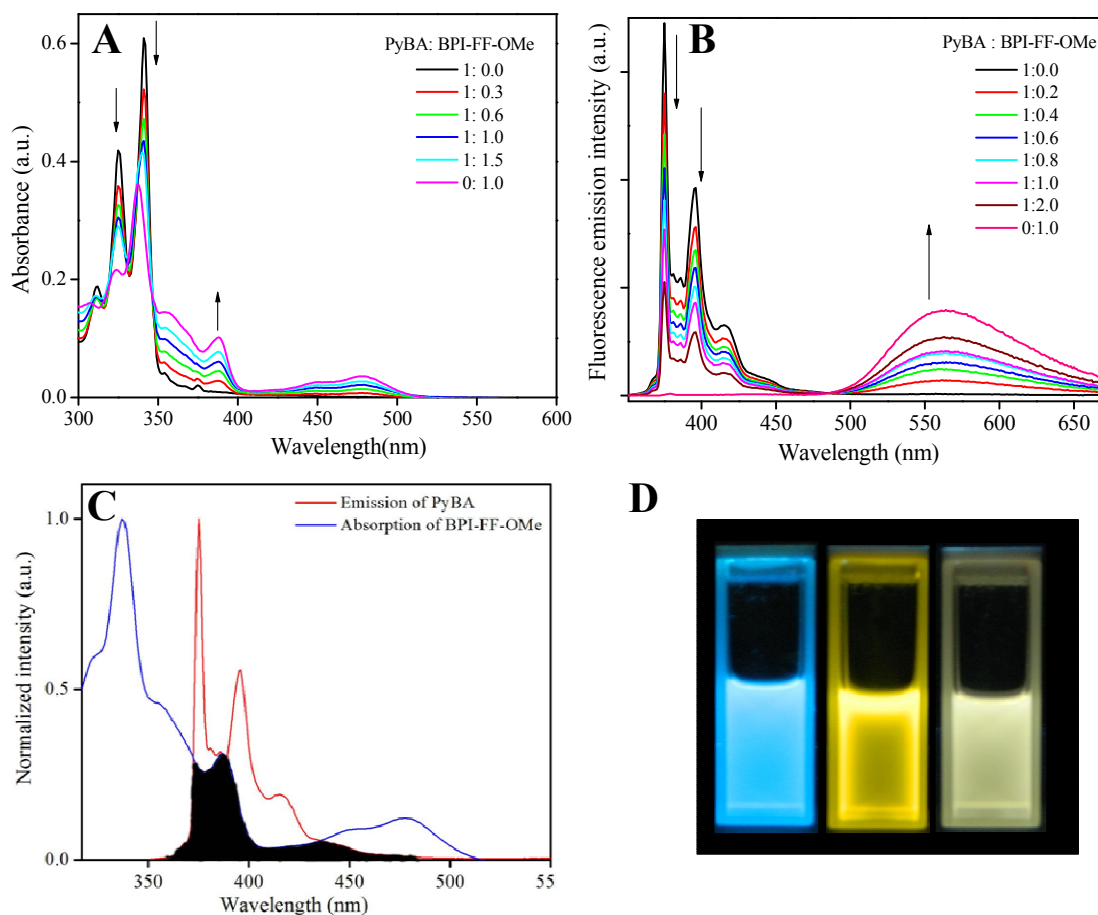


**Figure 10.** (A) UV-Vis and (B) fluorescence spectra of ( $1 \times 10^{-6}$  mol L $^{-1}$ ) of PyBA, BPI-FF-OMe and mixture of different equivalents of PyBA - BPI-FF-OMe in methanol respectively. (C) Spectral overlap region of emission spectrum of donor PyBA and absorption spectrum of acceptor BPI-FF-OMe. (D) Light emission of PyBA, BPI-FF-OMe and mixture of PyBA and BPI-FF-OMe (10:1) under 365 nm UV light.

## Table of Content

